


Modeling and Analysis of the Plastic Flow Curves of a Duplex Stainless Steel Using Artificial Intelligence

Leones Contini Jr.^a, Oscar Balancin^{a*} 

^aUniversidade Federal de São Carlos, Programa de Pós-Graduação em Engenharia Mecânica, 13565-905, São Carlos, SP, Brasil.

Received: February 11, 2022; Revised: May 11, 2022; Accepted: June 22, 2022

Determining the flow stress curves of metals and alloys in hot working conditions is essential for designers of metals forming processes. In this research, samples of a super duplex stainless steel with a ferrite matrix and dispersed austenite particles were deformed by torsion tests at temperatures ranging from 900 °C to 1200 °C and strain rates from 0.01 s⁻¹ to 10 s⁻¹. The level and shape of the plastic flow stress curves depend on the temperature and the strain rate and varies with the austenite volume fraction. When the two phases are deformed together, the marked difference in the softening behavior of austenite and ferrite leads to the uneven strain partitioning between these phases. As a consequence, the plastic behavior of this biphasic material is more complex than that of a single-phase material. A four columns spreadsheet was built using the experimental data obtained from the hot deformation testing. The first three columns contain the input data attributes (temperature, strain rate and strain) and the fourth the strength (stress) resulting from the material during deformation. These data were submitted to machine learning algorithms; initially in an artificial neural network with one hidden layer (ANN) and subsequently to a neural network with a specialist system (ANFIS). After the machine learning processes, the plastic flow curves were rebuilt and compared with those obtained experimentally. The ability of both algorithms to rebuild the plastic flow curves of the super duplex stainless steel were associated with changes in the shapes of the flow curves and microstructure evolution.

Keywords: Duplex Stainless Steel, Modeling Flow curves, Artificial Intelligence, Machine learning.

1. Introduction

Currently, transformations are taking place in the industrial production means to replace manual or mechanized operations by robotic procedures controlled by artificial intelligence (AI)^{1,2}. Mathematical models with different computational architectures are being formulated to accurately calculate operational parameters. Parameter values such as positions of the work piece, displacement speed of the tools, and the temperature of parts that are being deformed during hot metallurgical processing can be captured with good precision by sensors inserted in the machines and transferred to computer programs through of the internet of things (IoT). However, the plastic behavior of the materials cannot be directly determined in the production lines. Usually, the hot plastic behavior of metallic materials has been determined on a laboratory scale in the form of plastic flow stress curves^{3,4} and constitutive models are established to characterize the high temperature deformation behavior of metals and alloys.

To establish constitutive relationships between stress, strain, strain rate and temperature different approaches have been developed⁵. Some of them are phenomenological models: in this case an empirical model as a mathematical representation is used to described the correlation between the plastic parameters under a wide range of working conditions. For instance, taking into account that the flow

stress increases with higher strain rates and lower deformation temperatures, a relationship between peak stress, strain rate and temperature can be obtained using the hyperbolic sine constitutive equation proposed by Sellars and Tegart⁶. The constants n , A , α , and the apparent activation energy are determined at different strains and fitted by polynomial equations. Using the hyperbolic sine function and the relations attained between the constants and strain levels, flow curves can be successfully modeled. This procedure has been applied for different materials with good performance⁷⁻¹⁰.

Kingklang and Uthaisangsuk⁹ investigated duplex stainless steel grade 2507 conducting hot compression tests on heating: samples were heated just to deformation temperature and the obtained activation energy was 689.5 kJ/mol. However, some works have found different values for activation energy at different temperatures. Farnoush et al.¹¹ investigated the 2205 duplex stainless steel by compression tests and found different activation energies; 554 kJ/mol at lower temperatures and 310 kJ/mol at higher temperatures. Iza-Mendia et al.¹² found two values for activation energy at two different temperature ranges conducting torsion and plane strain compression tests after long soaking time (1 hour); the relative long soaking time assure that the equilibrium microstructure is reached before testing. One of the authors of this research also found different activation energies conducting hot torsion tests in a duplex stainless steel¹³. The tests were carried out on cooling and the difference was

*e-mail: balancin@ufscar.br

associated with the change in the austenite volume fraction due to the decrease of deformation temperature.

Another procedure to set constitutive models is the use of physically-based models which allow for a precise definition of deformation mechanisms over a wide range of working conditions supported by some physical assumptions. Mainly, models related to physical parameters such as dislocation density and grain size. Such modeling must describe material flow stress evolution regarding microstructure, hardening mechanisms, softening mechanisms and grain boundary mobility. This approach has been applied for different materials with good performance¹⁴⁻¹⁷. For instance, it is well known that single-phase ferritic stainless steels soften by intense recovery during straining^{18,19} while single-phase austenite, with relative low stacking fault energies, soften by dynamic recrystallization, after some amount of work hardening and dynamic recovery^{20,21}. When deformation is conducted with constant temperature and strain rate, the flow stress increases in the initial work hardening regime and then becomes constant in the ferrite phase; in contrast, the stress experiences a maximum before decreasing to a steady state in the austenite phase²². Materials with well-known and parameterizable plastic behaviors allow the application of physically-based models such as generation and annihilation of dislocations and the Avrami equation to describe their behavior mathematically.

However, there are materials that have more complex plastic behavior such as two-phase alloys as duplex stainless steels. Under hot processing conditions, ferritic-austenitic duplex stainless steels consist of austenite particles embedded in a ferrite matrix. When the two phases are deformed together, the marked difference in the softening behavior of austenite and ferrite leads to the uneven strain partitioning between these phases. The deformation distribution is no longer uniform, with deformation concentration in the softer alpha phase at the beginning of the deformation. At this stage, strain is mostly accommodated by softer phase and dynamic recovery in ferrite is accelerated with a gradual increase in misorientation between neighboring subgrains²³ and gradually converted during straining into high-angle boundaries through continuous absorption of dislocations²⁴. At higher straining levels, load transfers to austenite giving rise to the build-up of dislocation until dynamic recrystallization starts. However, owing to limitation in the number of austenite/austenite boundaries and limited strain transferred to austenite, the evolution of dynamic recrystallization in austenite is markedly suppressed^{12,25}. As a consequence, depending on the mechanisms that are controlling the plastic deformation, the flow stress curve takes different shapes²⁶.

Besides the hardening and softening mechanisms acting in each one of constituent phases and the strain partitioning, the plastic behavior of two phases stainless steel depends on the volume fraction, distribution and morphology of austenite in the ferrite matrix and on the nature of the interface between these phases. The volume fraction of austenite depends on deformation temperature,

increasing as temperature decreases^{26,27}. During straining, the deformation gradients and the flow stresses can also be altered by the action of mechanisms such as local shear or sliding of the interphase boundary¹² and the change of the coherence between austenite and ferrite interface^{13,26}. After some amount of deformation, with the transfer of stress to the austenitic phase, fragmentation of these particles can take place. Consequently, the construction of physically-based constitutive models to describe the plastic behavior of these materials needs further investigations.

Recent advances in machine learning processes engendered a realistic alternative for modeling the plastic flow stress curves of metals and alloys using artificial neural network (ANN) techniques. ANN can learn from examples and recognize paths in a series of inputs and outputs data without any prior knowledge of their natures and interrelations. This method has been applied for different materials with good performance²⁸⁻³⁴. Also, one kind of artificial intelligence technique combining neural networks and the capabilities of the fuzzy logic inference system learning (ANFIS) can be used to establish accurate mapping relations between inputs and outputs data³⁵. Fuzzy systems use a mathematical method to introduce the subjective human knowledge in the real processes. ANFIS has been applied for different materials with good performance^{36,37}. Some of these research compare the fitness achieved by AI with that attained with phenomenological models^{29,31,34} and other with the physically-based constitutive model³⁶. Independent of the model type used the attained data indicated best fitness with AI. Since these algorithms postulate no specific mathematical expression and can be easily established based on experimental data, it is expected to be possible to model and predict the high temperature deformation behavior of the super duplex stainless steel without to consider the evolution of austenite volume fraction as temperature decreases.

2. Material and Procedures

The material used in this work was a super duplex stainless steel - UNS S32760 - whose chemical composition is indicated in Table 1.

2.1. Mechanical tests

Mechanical tests were conducted on a horizontal hot torsion testing machine, in which, a microcomputer was attached through interfaces allowing machine-computer intercommunication, control of the tests and data acquisition. The samples had reduced torsion gage sections 12 mm in length and 6 mm in diameter. When a torsional moment is applied in the sample, the state of stress developed in the central region can be represented by Figure 1. Tensile stress (σ_1) and compression stress (σ_3) are equal in magnitude to the maximum shear stresses (τ_{max}), and are oriented at an angle of 45° with the direction of these stresses, that is, with the longitudinal axis of the sample. The stress acting on the

Table 1. Chemical composition of the UNS S32760 stainless steel (mass%)

C	Si	Mn	Cr	Ni	Mo	W	Cu	N	Fe
0.02	0.25	0.54	25.18	7.04	3.57	0.53	0.55	0.23	Bal.

normal plane of these stresses (intermediate stress $-\sigma_2$) is equal to zero.

Torsion moment required to deform the material was measured by a torsion cell coupled to the machine and sent to the software. The true stress was calculated using the equation:

$$\sigma = \frac{\sqrt{3} \cdot M}{2 \cdot \pi \cdot R^3} (3 + m + n)$$

where M is the torsion moment, R is the radius of the specimen and m and n are the sensitivity coefficients of the material to the strain rate and work hardening, respectively.

The state of strain present when a torsion effort is applying in the sample is shown in Figure 2. Before applying the torsion effort, the elements drawn on the sample surface are presented with parallel faces to each other (Figure 2a). After applying a torsional moment, the elements deform and one of the diagonals elongates while the other is reduced, transforming each initial square into a lozenge (Figure 2b).

Twist angle were measured by an encoder coupled to the machine and sent to the software. The true strain was calculated using the equation:

$$\varepsilon = \frac{R \cdot \theta}{\sqrt{3} \cdot L}$$

where L is the useful specimen length, R is the specimen radius and θ the rotation angle of the machine. The strain rate is calculated by dividing the strain by the total testing time.

The samples were heated by means of an infrared radiation furnace mounted directly on the testing machine. Chromel-alumel thermocouples welded at surface of the samples were used for temperature measurement and control. On carrying out the tests, samples were heated to 1200 °C with a rate of 2°C/s and maintained at this temperature for 10 minutes in an argon atmosphere. After this, the samples were cooled until the deformation temperatures with a rate

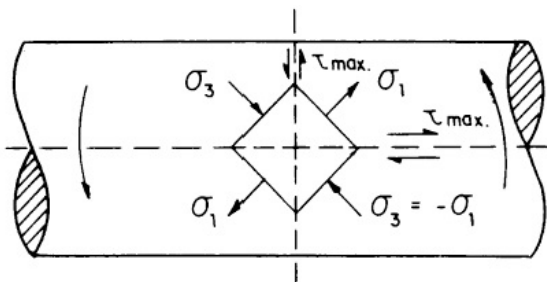


Figure 1. Stress state in the central region of a solid circular specimen under torsion at its ends

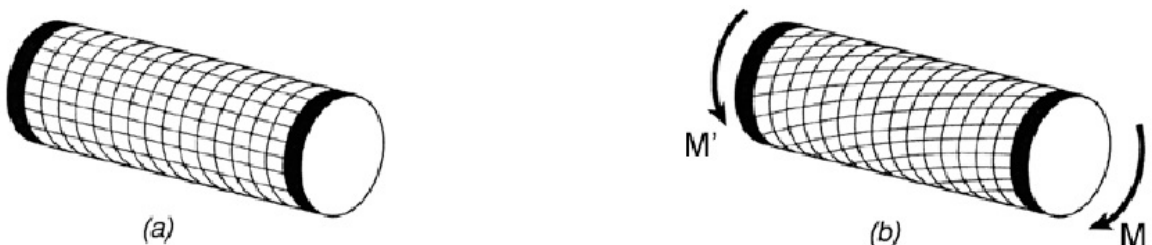


Figure 2. Central region of a sample submitted to a torsion effort. (a) Before the effort to be applied and (b) after the applied torque

of 1°C/s and maintained at these temperatures for 30 seconds to eliminate thermal gradients. Hot torsion tests were performed at 900 °C, 1000 °C, 1100 °C and 1200 °C with strain rates of 0.01, 0.1, 1 and 10 s⁻¹. These temperatures, heating and cooling rates, and the strain rates were imposed and controlled by the software.

2.2. Neural networks modelling for predicting true stresses of the super duplex steel

In this work, two machine learning algorithms were used: shallow artificial neural network with one hidden layer and the combination of an ANN with fuzzy logic, creating an adaptive neuro-fuzzy inference system (ANFIS).

2.2.1. Artificial Neural Network

Artificial neural network is a mathematical and/or computational model that mimics the structure and functional aspects of a biological neural network. An ANN consists of a set of interconnected artificial neurons (nodes) that process information using computational methods. Neural network is hierarchical with neurons grouped in different layers designed as an input layer, hidden layers and output layer (see Figure 3). Analogously to the human brain, ANNs have the ability to interact with and adapt to the external environment. An ANN can learn from examples and recognize paths in a series of inputs and outputs data without any prior knowledge of their natures and interrelations. All that is needed is a collection of representative examples of the desired mapping.

Training of a neural network model consists of adjusting the weights associated with each connection between the neurons. In the feedforward process, each incoming signal spread out along the network until the end layer of neurons in the output layer. In the final layer, the output value is generated and then compared with the actual (target) value. The difference between experimental and the calculated value is determined, the back propagation algorithm adjusts the network weights so that the next calculated output will be closer to the target value. A feedforward back propagation (BP) artificial neural network with Levenberg – Marquardt training algorithm was applied to predicted the flow stress of the experimental duplex stainless steel. The learning is based on gradient descent algorithm and hence requires the activation function to be differentiable, and so a logistic sigmoidal function was employed as the activation function. A detailed description of the algorithms used in this study is beyond the scope of the present paper and it can be found elsewhere³⁸.

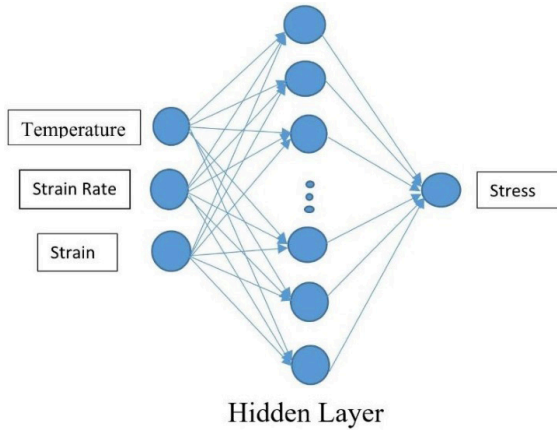


Figure 3. Schematic illustration of network architecture with one hidden layer

Alongside the activation functions, the number of neurons in the hidden layer define the architecture of the ANN. The number of neurons in the hidden layer is determined by experience, and trial and error. In this research, an experiment was conducted changing the number of neurons from 1 to 25 in the hidden layer to determine the best resolution.

For efficient training of the neural network model, the data need to be normalized before entering the ANN. Differences on the data values due to different units used in each parameter can result in deviation in the training results, because small and large magnitudes mixed experimental data will confuse the learning process. As a consequence, both input data and output data were normalized in the range of 0 - 1. The used method of normalization was:

$$X_i = 0.1 + 0.8x \left(\frac{X - X_{\min}}{X_{\max} - X_{\min}} \right)$$

where X is the original data, X_{\min} the minimum value of X , X_{\max} the maximum value of X , and X_i the normalized data of the corresponding X . Logarithmic values of strain rates were used here because this parameter changes severely, from 0.01 to 10 s^{-1} .

To validate the generalization capability of the newly trained ANN, a set of test data not used in the training stage was supplied as the inputs. In this work, all data set was divided in three set: larger part of the data was randomly selected to train the ANN model and two smaller data sets were used to validate and test the predictability of the newly trained ANN. The network was considered well trained if the error between the predicted and actual output values were considered by the user as insignificant.

The prediction results are quantified using statistical parameters to evaluate the prediction accuracy of the ANN model. Statistical parameters are mainly introduced: mean absolute percentage error (MAPE), root means square error (RMSE) and correlation coefficient (R^2).

$$MAPE = \frac{\sum_1^N \left| \frac{E_i - P_i}{E_i} \right|}{N} \times (100)$$

$$RMSE = \left[\frac{1}{N} \sum_1^N (E_i - P_i)^2 \right]^{\frac{1}{2}}$$

$$R = \frac{\sum_1^N (E_i - \bar{E})(P_i - \bar{P})}{\sqrt{\sum_1^N (E_i - \bar{E})^2} \sqrt{\sum_1^N (P_i - \bar{P})^2}}$$

where E is the experimental value of the stress and P is the predicted value by the ANN model, and N is the number of data points. \bar{E} and \bar{P} represent the mean values of the measured and predicted values of E and P .

2.2.2. Adaptive neuro-fuzzy inference system

The data volume is a critical condition for properly conducting the machine learning process and obtaining consistent results applying an ANN. However, the necessary quantity of data is not always available. An alternative is to adapt a specialist system to the neural network. The use of fuzzy logic in a neural network is a methodology that has shown good results, allowing simulation and machine learning with a smaller data volume. Fuzzy systems employ a mathematical method to introduce the subjective human knowledge in the real processes. This is a way to manipulate practical knowledge with some level of uncertainty. The behavior of such system is described through a set of fuzzy rules, like: IF <premise> Then <consequent> that uses linguistic variables with symbolic terms³⁹.

The neural networks, that have efficient learning algorithms, have been presented as an alternative to automate or to support the development of tuning fuzzy systems. Neural networks introduce its computational characteristics of learning in the fuzzy systems and receive from them the interpretation and clarity of systems representation. The combination of an ANN with fuzzy logic creates an adaptive neuro-fuzzy inference system (ANFIS) with five layers and implements a Sugeno FIS procedure³⁵. The first layer is responsible for the mapping of the input variable relative to each membership functions (MFs). The second layer executes the T-norm of the antecedent part of the fuzzy rules. The third layer normalizes the membership functions. The fourth layer calculates the consequent parameters, and finally the last layer computes the overall output as the summation of all incoming signals³⁸ (see Figure 4). Since the number of layers for ANFIS is fixed as 5, when the number of membership functions is determined, the number of node in every layer is established. Thus, after determining the number of MF, the type of MF should be determined to completely proven the ANFIS.

The neuro adaptive inference system generates a procedure to find the data set that appropriately adjusts the pertinence functions to the input and output data. This is done using the backpropagation (BP) algorithm and the least square method to obtain the best membership functions. Although the fuzzy inference system uses linguistic variables in the form of 'if-then', the possibility of adjustment under new situations is introduced in ANN training. ANFIS provides the best advantages that exist in fuzzy logic and neural network techniques in a single tool.

3. Results

3.1. Plastic flow curves

Figure 5 shows the plastic flow curves obtained experimentally. These curves have the typical shape of the hot mechanical behavior of steels; the stress increases with deformation to a maximum and then decreases. It can be seen in this figure that samples deformed at low temperatures and with high strain rates failed with deformations close to 1.0 – 1.5. On the other hand, samples deformed at high temperatures and low strain rates supported larger deformations; at 1200 °C with strain rates from 0.01 to 1 s⁻¹ the material did not fail even though with deformation of 3.0. However, the steady state of stresses in large strains has not been observed.

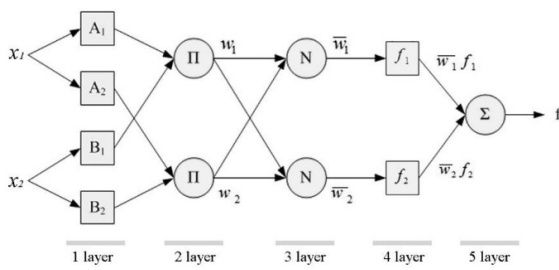


Figure 4. Schematic illustration of an ANFIS network architecture.

From the experimental data shown in Figure 5, it is worth noting that there are significant differences in the shape of these curves compared with those presented by single-phase materials that soften by dynamic recovery and/or dynamic recrystallization. Also, it can be noticed changes in the mechanical behavior of the material as the deformation conditions were altered; the shape of the plastic flow curve assumes two distinct forms. At low temperatures and/or high strain rates, the curves have a rounded shape, as can be seen at 900 °C and 1000 °C with strain rates of 1.0 and 10 s⁻¹. At high temperatures and/or low strain rates, the stress increases almost linearly to a maximum at the beginning of the straining. On reaching the maximum, it may or may not have a range of straining with constant stress, after which the stress decrease.

In this research, a typical laboratory deformation mode was used, whose stress and strain states are well known. Before the samples of duplex stainless steel being deformed, the austenite particles were aligned with the axis of the specimens. When the material was strained, these particles rotated tending to align with the maximum shear stress direction and transfer of stress and strain to austenite took place. As a result, the austenite particles were elongated due to the action of the principal tensile stress (σ_1) and laterally compressed with the action of the principal compressive stress (σ_3), tending to agglomerate, as shown in Figure 6.

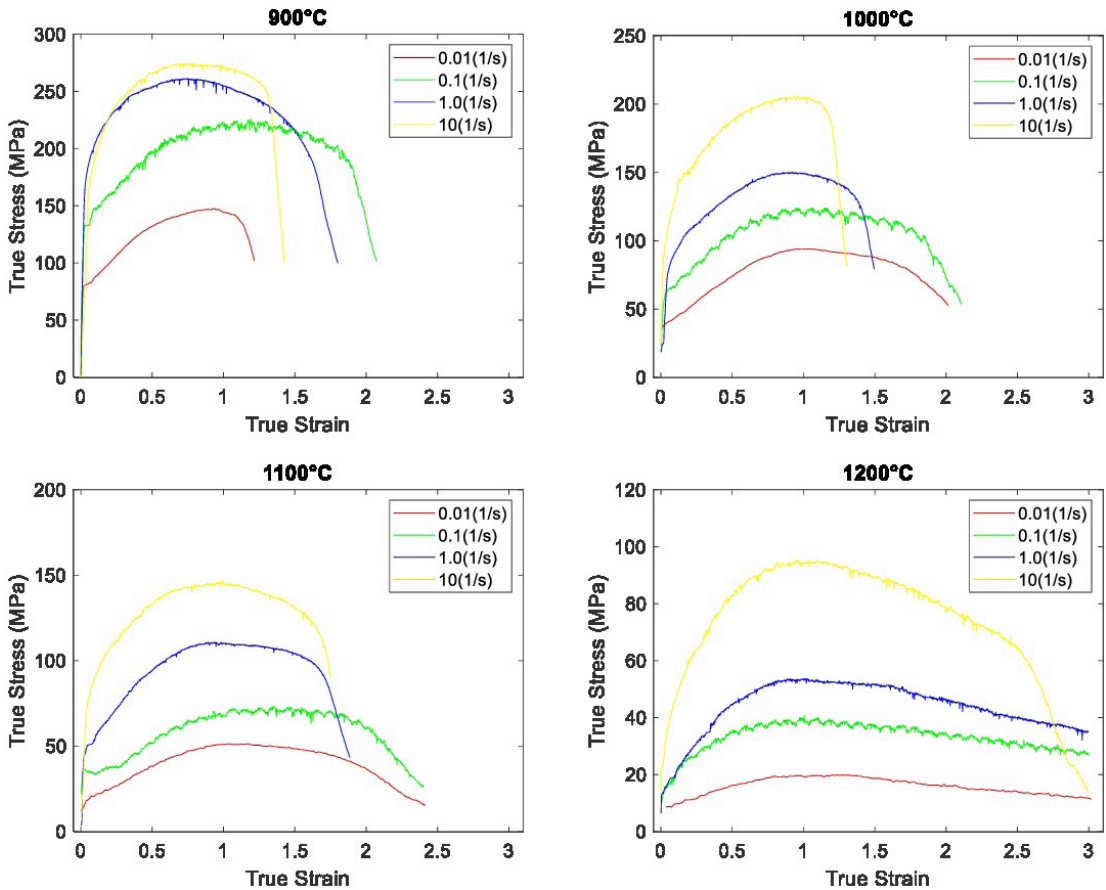


Figure 5. Plastic flow curves obtained in hot torsion tests.

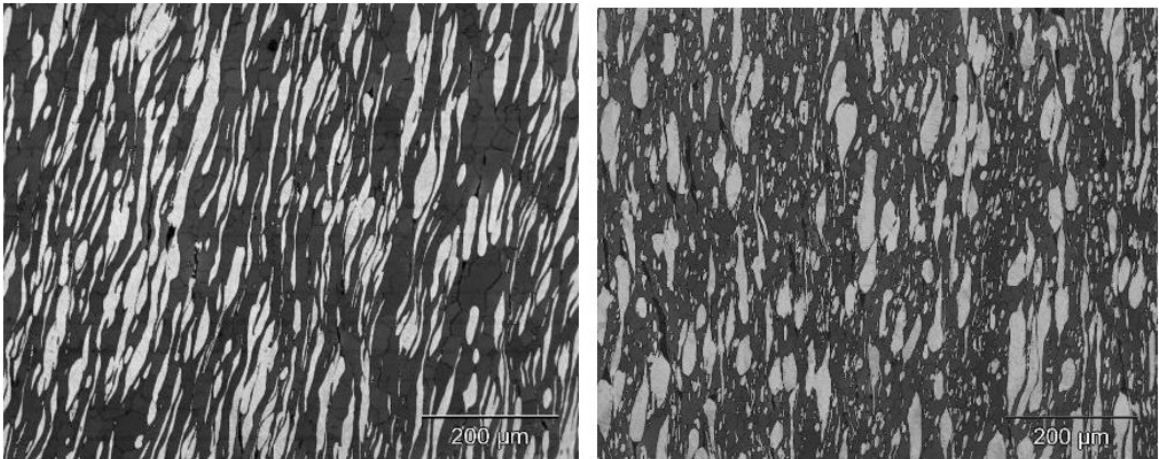


Figure 6. Microstructure of samples deformed with 1.0 s^{-1} at (a) 1200°C and (b) 1000°C .

In this figure one can observe changes in the distribution and volume fraction of the austenite particles. At lower temperature not only austenite particles that were present during reheating but also particles precipitated during cooling and deformation can be observed in Figure 6b; small particles between larger ones that came from reheating. As a consequence, the volume fraction of austenite changed from smaller amounts of austenite at high temperatures to volume fractions close to those of ferrite when the deformation temperature is decreased²⁶.

From the data obtained in the experimental tests, a worksheet containing the input attributes and the output values was built. The values of temperature, strain rate and deformation were considered input and the values of the applied stresses by the machine were the output values. However, it is worth nothing in Figure 5 that the flow curves display not only the plastic region but also some extension after the material had failed. As the aim of this study was to simulate the plastic behavior, it was necessary to use only the plastic region as the initial data set. The table was arranged with the increasing of the temperature and strain rate; 900°C with strain rate increasing from 0.01 to 10 s^{-1} , 1000°C with strain rate increasing from 0.01 to 10 s^{-1} and so on. In this case, a matrix with four columns and with 10 158 data points were assembled.

3.2. ANN predictions

In the supervised machine learning process the software (algorithm) creates a model that describes the relationship between the input and the output data. With this model, the output data is calculated and compared with the experimental values. By comparing these data, errors in the learning process are determined. In this exercise, the data set was divided into three sets: 70% for training, 15% for validation and 15% for test. To design the number of neurons in the hidden layer, the evolution of the root mean squared error (RMSE) in the shallow neural network applied to duplex stainless steel altering the number of neurons in the hidden layer was determined and are displayed in Figure 7. The RMSE values decreased as the number of neurons increases: for small number of neurons the slope is larger, however for 18 or

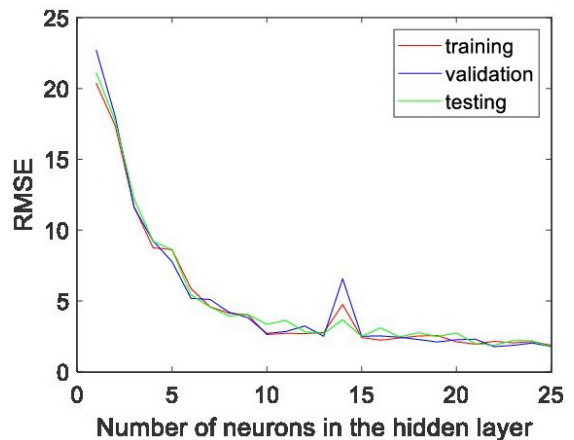


Figure 7. Evolution of the root mean square error with the number of neurons in the hidden layer.

more neurons the error is basically constant considering the training, validation and testing data sets. This information together with a logistic sigmoidal activation function defines the architecture of the ANN algorithm ($3 \times 18 \times 1$) used in this research.

Once defined the ANN architecture, this was used to predict the plastic behavior of the duplex stainless steel. Flow stress curves predicted by the ANN model together with the experimental curves are displayed in Figure 8. In this diagram, all (16) flow stress curves of the duplex stainless steel were plotted together using the full data set. By comparing the calculated and experimental data one can see that the ANN model accurately describe the plastic behavior of the duplex stainless steel during hot deformation, indicating that the machine learning process was successful.

The deviation between calculated and measured curves was analyzed using statistical parameters and are displayed in Table 2. The mean residuals between the measured data point and the calculated one was 2.176 MPa for the training experiments, which represents a percentage error of the 1.552% and the data attained by ANN represents 99.9% of

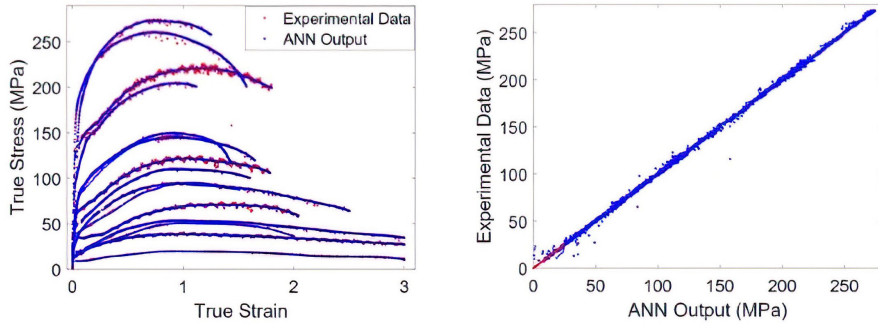


Figure 8. (a) Results of the machine learning process with ANN and (b) predicted and experimental values correlation.

Table 2. Statistical parameter values determine from the learning process.

	RMSE (MPa)	MAPE (%)	R ²
Training	2.176	1.552	0.999
Validation	2.163	1.457	0.999
Test	2.415	1.619	0.999

the variation in the relationship between stress and strain obtained experimentally. Also, the values of statistical parameters determined are close for training, validation and test data sets. These values indicate that the model has a strong prediction ability and high precision for determine the flow stress in hot deformation, even for a material that the shape of flow stress depends on the other parameters such as the volume fraction of the second phase that was not considered in this study.

3.3. ANFIS results

Determination of the appropriate ANFIS architecture to analyze the flow stress curve predictions of the duplex stainless steel were conducted varying the number and type of membership functions (MF). The type of MF for three input parameters were selected as triangle-shape membership function (trimf), bell-shape membership function (gbellmf) and gauss-shape membership function (gaussmf). Since the product of the three membership functions determine the number of rules, this parameter was used to indicate the evolution of the ANFIS architecture.

From Figure 5 one can see that the flow stress curves were determined with temperature and strain rate constants at four different levels for which one, and the strain varied continuously from 0 to 3.0. Thus, it is expected that a good choice for MFs number can be four for temperature and four for strain rate. Also, the large ductility difference between flow stress curves suggests that is necessary a larger number of memberships functions for strain. The RMSE trend for the three variables from ANFIS model using different combination of number and types of MF are shown in Figure 9.

One can see in this figure that the RMSE decreases as the number of rules increases. Since the number of MFs for temperature and strain rate was constant, increasing the number of rules means increases the number of MFs for

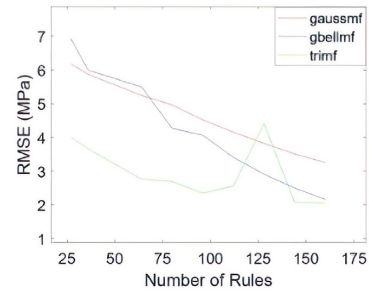


Figure 9. Evolution of the RMSE with the architecture of the ANFIS.

strain. The combination of three trimf MFs indicates the minimum value of the RMSE, although this curve shows an increases in the RMSE when the number of rules was 128. Also, visually was noted that when the trimf was used as the MF for strain the data deviation concentrated just in one point, distorting the flow curves. When the gbellmf or gaussmf MF types were applied for strain, combination with others MF types result in very small difference in the RMSE. As a consequence, the combination of three gbellmf was used to build the architecture of the ANFIS.

Building an ANFIS with (4 4 10) and (gbellmf, gbellmf, gbellmf) MFs, the duplex stainless steel data set was trained. In this work, the data set was divided in three sets: 70% of the data was randomly selected to train the ANFIS model and two data sets of 15% were used to validate the predictability and test of the newly trained ANFIS. The calculated output together with the experimental data set are presented in Figure 10. This figure indicates that the deviations between experimental and calculated values are relatively small. However, it is worth noting that there are some differences in the fitting of the curves: the fitting is better at higher temperatures and smaller strain rates (smaller stresses) than in lower temperatures and higher strain rates (higher stresses).

The ANFIS trained model was used to validate the generalization capability of the algorithm. The deviation between calculated and measured data was analyzed using statistical parameters and are displayed in Table 3.

The mean residuals between the measured data point and the calculated one is 2.071 MPa for the training experiments, which represents a percentage error of the 2.048% and the data attained by ANFIS represents 99.9% of the variation in the relationship between stress and strain determined experimentally. Comparing this spreading with that attained in the ANN (Table 2), one can see that both errors of the training data are very close. However, the error for validation and test data sets are something greater as shown in Table 3.

The model established by the machine learning process was used to predict stress values in conditions where no experimental measurements had been done. Figure 11a displays the forecasted stress vs. strain curves for deformation at 950 °C with strain rate of 5.5 s⁻¹ (950/5.5), 1050 °C with strain rate of 0.055 s⁻¹ (1050/0.55) and 1150 °C with strain rate of 0.055 s⁻¹ (1150/0.055). These deformation conditions represent

Table 3. Statistical parameter values determine from the learning process

	RMSE (MPa)	MAPE (%)	R ²
Training	2.071	2.048	0.999
Validating	2.595	5.139	0.999
test	2.638	5.205	0.999

intermediate levels between the experimental curves at 900 °C with strain rate of 10 s⁻¹ (900/10), 1000 °C with strain rate of 1 s⁻¹ (1000/1), 1100 °C with strain rate of 0.1 s⁻¹ (1100/0.1) and 1200 °C strain rate of 0.01 s⁻¹ (1200/0.01). Visually, one can say that the predicted curves assume intermediate values between the experimental ones. To check this observation, Figure 11b shows the evolution of the stresses for the seven temperatures with strain of 0.5. Together with data attained with ANFIS are presented data calculated with ANN. It is clear that both models predict well the stress evolution.

Another interesting feature of the ANFIS algorithm is that it allows to view alone or simultaneously the dependence of the output values with the input attributes. Figure 12 shows, as an example, the stress dependence on temperature and strain rate. It can be seen in this figure that the stress increases with the strain rate and decreases with the temperature continuously and these changes are not symmetrical. By the shape of this figure it can be seen that the variation of 100 °C on the temperature scale has increased more the stress than the variation of an order of magnitude in the strain rates in the interval used in the experiments.

In this figure, the surface was determined for deformation of 0.5. The top point of this figure represents a straining of 0.5 at 900 °C with strain rate of 10 s⁻¹ and the value of

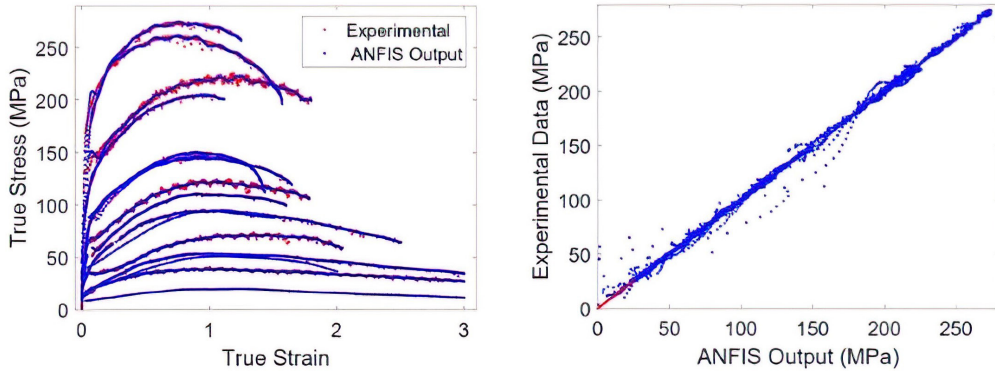


Figure 10. (a) Results of the machine learning process with ANFIS modeling and (b) scatter map of the predicted and measured true stresses.

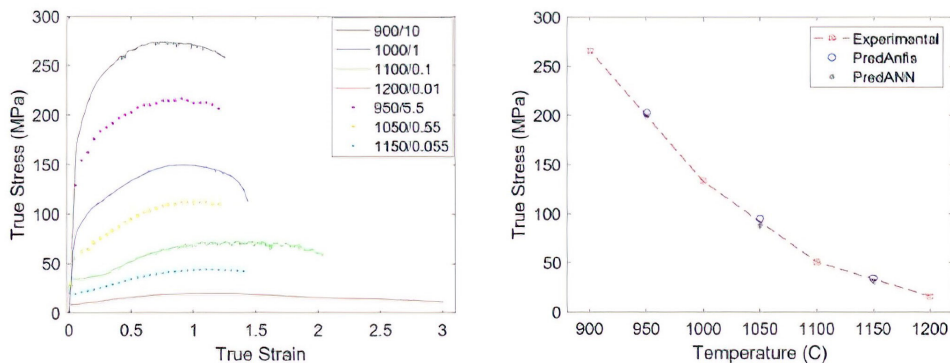


Figure 11. Predicted stress values for intermediate deformation conditions.

stress read in this graph is 265 MPa. The lowermost point represents a straining of 0.5 at 1200 °C and strain rate of 0.01 s⁻¹ and the value reached is 17 MPa. Comparing these stresses with those presented in Figure 11b one can see that they are very close (266 and 17.5 MPa). The smallest line linking both points represents the curve presented in Figure 11b. Also, one can see that this figure describes the variations of the temperature and of the strain rate for all possible deformation conditions with straining of 0.5. It is worth bearing in mind that the deviations between the actual values and the calculated ones are described by the statistical parameters presented in Table 3.

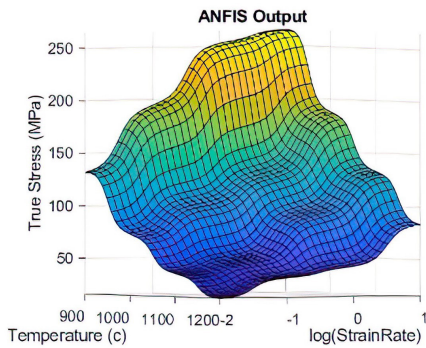


Figure 12. Dependence of stress with temperature and strain rate for a strain equal 0.5.

4. Discussion

The performed machine learning processes, with shallow neural network and with fuzzy logic displayed in Figures 8 and 10, indicate that the fit between the experimental and the calculated data was satisfactory. In both cases, the correlation coefficient was 0.999, indicating that R² is close to 100%; the predicted curves represent well the experimental ones. It is clear that both models predict well the true stress evolution of the duplex stainless steel during plastic deformation at high temperature and high strain rate. To illustrate this statement, experimental curves and outputs of the proposed models are compared in the graphs presented in the Figure 13.

One can see in this figure that the flow stress curves predicted by both techniques are very similar to the experimental ones. However, comparing the curves displayed in this figure, one can see that the fitting of experimental and predicted curves are something better when it was conducted by ANN algorithm. Visually the fitting by ANN is very similar for all curves and the statistical parameters assume smaller values than that for ANFIS predictions. On the other hand, it is possible to see that the scattering between the measured points and the calculated values are larger in the curves with low ductility when the fitting was conducted by ANFIS (Figures 10 and 13).

During the hot working process, the material flow stress curve depends on the strain, strain rate, temperature and the initial microstructure. Bearing in mind that all samples were reheated to the same temperature and the deformation begun

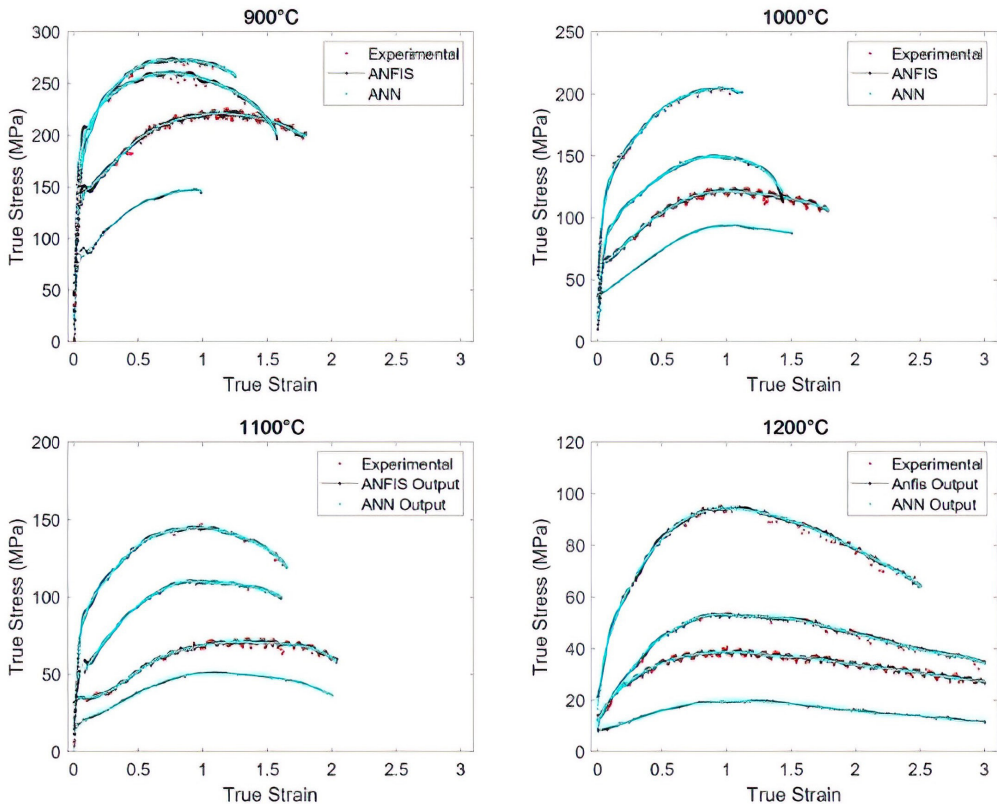


Figure 13. Plastic flow curves determined experimentally, ANFIS outputs and ANN outputs.

after controlled cooling to different deformation temperatures, different microstructures were present during deformation, as depicted in Figure 6. At high temperatures, when the austenite volume fraction is lower and the mean free path between austenite particles is larger, the deformation is concentrated on the softer ferrite, as can be seen in Figure 6a. In this case there was flow of ferrite around and parallel to the austenite particles. By decreasing the test temperature, the volumetric fraction of austenite increases due to precipitation of new austenite particles (Figure 6b), reducing the spacing between the particles. When the material was strained, stress was transferred to austenite.

In previous works two different behaviors of duplex stainless steels under hot work conditions have been observed when the strain rate and the deformation temperature are changed; this class of steel exhibit larger activation energy when strained at higher Z (Zener-Hollomon) parameter (higher strain rates and lower temperatures) than when deformed at higher temperatures and lower strain rates (11,13). At low Z values ferrite accommodates strain and dynamic recovery is the softening mechanism that is acting, while at high Z values austenite controls the deformation and dynamic recrystallization can take place. Also, in addition to dynamic recrystallization, slip of phase contours or even though fragmentation of austenite particles can take place in this condition.

Since the machine learning process is conducted determining the best weights for each synapse (link between neurons), ANN does not need to know the physical mechanisms that act during hot deformation, allowing best fitting of the data. On the other hand, the ANFIS modeling is conducted using fuzzy logic, which utilizes a mathematical method to introduce the subjective human knowledge in the real processes. In this case, one can speculate that some rules do not adjust well to microstructure changes caused by the increase of austenite volume fraction, as a consequence of the decrease of deformation temperature, that was not considered as input in this machine learning process.

5. Conclusions

The use of AI allows satisfactory modeling of the hot plastic flow curves of super duplex stainless steel whose mechanisms that act during hot deformation are not fully known. The machine learning process generates models that establish relationships between the input and output attributes allowing the prediction of values for data points not measured experimentally. The fit of the experimental and predicted curves for duplex stainless steel is somewhat better when performed by the ANN algorithm.

The mean residuals between the measured and the calculated data points applying the ANN algorithm was 2.2 MPa for the training experiments, which represents a percentage error of the 1.6% and the data attained by ANN represents 99.9% of the variation in the relationship between stress and strain obtained experimentally. Also, the values of statistical parameters determined are close for training, validation and test data sets.

When the ANFIS algorithm was applied, the mean residuals between the measured and calculated data for training are similar to those obtained by the ANN. The average residuals

are very close for validation and testing, but somewhat higher than those for training: 2.6 MPa for the validation experiments, which represents a percentage error of 5.1% and the data obtained by ANFIS represents 99.9% of the variations in the relationship between stress and strain determined experimentally.

6. References

- Zhong RY, Xu X, Klotz E, Newman ST. Intelligent manufacturing in the context of industry 4.0: a review. *Engineering*. 2017;3(5):616-30.
- Branca TA, Fornai B, Colla V, Murri MM, Streppa E, Schröder AJ. The challenge of digitalization in the steel sector. *Metals*. 2020;10(2):288.
- Lourenço NJ, Jorge AM Jr, Rollo JMA, Balancin O. Plastic behavior of medium carbon vanadium microalloyed steel at temperatures near $\gamma \rightarrow \alpha$ transformation. *Mater Res*. 2001;4(3):149-56.
- El-Shenawy EH. Physical simulation of thermo-mechanical processing of metallic alloys using gleeble system. *Mater Today Proc*. 2020;28:998-1004. <http://dx.doi.org/10.1016/j.matpr.2019.12.339>.
- Lin YC, Chen X-M. A critical review of experimental results and constitutive descriptions for metals and alloys in hot working. *Mater Des*. 2011;32(4):1733-59.
- Sellars CM, Tegart WJ. La relation entre la résistance et la structure dans la déformation à chaud. *Mem Sci Rev Metall*. 1966;63:731-46.
- Xiao Y-H, Guo C. Constitutive modelling for high temperature behavior of 1Cr12Ni3Mo2VNbN martensitic steel. *Mater Sci Eng A*. 2011;528(15):5081-7.
- Lin YC, Wen D-X, Deng J, Liu G, Chen J. Constitutive models for high-temperature flow behaviors of a Ni-based superalloy. *Mater Des*. 2014;59:115-23.
- Kingklang S, Uthaisangsuk V. Investigation of hot deformation behavior of duplex stainless steel grade 2507. *Metall Mater Trans, A Phys Metall Mater Sci*. 2017;48(1):95-108.
- Kumar N, Kumar S, Rajput SK, Nath SK. Modelling of flow stress and prediction of workability by processing map for hot compression of 42CrNi steel. *ISIJ Int*. 2017;57(3):497-505.
- Farnoush H, Momeni A, Deghani K, Mohandesi JA, Keshmiri H. Hot deformation characteristics of 2205 duplex stainless steel based on the behavior of constituent phases. *Mater Des*. 2010;31(1):220-6.
- Iza-Mendia A, Piñol-Juez A, Urcola JJ, Gutiérrez I. Microstructural and mechanical behavior of a duplex stainless steel under hot working conditions. *Metall Mater Trans, A Phys Metall Mater Sci*. 1998;29:2975-86.
- Balancin O, Hoffmann WAM, Jonas JJ. Influence of microstructure on the flow behavior of duplex stainless steels at high temperature. *Metall Mater Trans, A Phys Metall Mater Sci*. 2000;31(5):1353-64.
- Laasraoui A, Jonas JJ. Prediction of steel flow stresses at high temperatures and strain rates. *Metall Trans, A, Phys Metall Mater Sci*. 1991;22(7):1545-58.
- Medina SF, Hernandez CA. Modelling of the dynamic recrystallization of austenite in low alloy and microalloyed steels. *Acta Mater*. 1996;44(1):165-71.
- Jorge AM Jr, Balancin O. Prediction of steel flow stress under hot working conditions. *Mater Res*. 2005;8(3):309-15.
- Jonas JJ, Quelennec X, Jiang L, Martin É. The Avrami kinetics of dynamic recrystallization. *Acta Mater*. 2009;57(9):2748-56.
- Longfei L, Wangyue Y, Zuqing S. Dynamic recrystallization of ferrite in a low-carbon steel. *Metall Mater Trans, A Phys Metall Mater Sci*. 2006;37(3):609-19.

19. Castan C, Montheillet F, Perlade A. Dynamic recrystallization mechanisms of an Fe–8% Al low density steel under hot rolling conditions. *Scr Mater*. 2013;68(6):360-4.
20. Dehghan-Manshadi A, Hodgson PD. Dependency of recrystallization mechanism to the initial grain size. *Metall Mater Trans, A Phys Metall Mater Sci*. 2008;39(12):2830-40.
21. Beladi H, Cizek P, Hodgson PD. On the characteristics of substructure development through dynamic recrystallization. *Acta Mater*. 2010;58(9):3531-41.
22. Jorge AM Jr, Regone W, Balancin O. Effect of competing hardening and softening mechanisms on the flow stress curve modeling of ultra-low carbon steel at high temperatures. *J Mater Process Technol*. 2003;142(2):415-21.
23. Cizek P, Wynne BP. A mechanism of ferrite softening in a duplex stainless steel deformed in hot torsion. *Mater Sci Eng A*. 1997;230(1-2):88-94.
24. Haghdadi N, Cizek P, Beladi H, Hodgson PD. Dynamic restoration processes in a 23Cr-6Ni-3Mo duplex stainless steel: effect of austenite morphology and interface characteristics. *Metall Mater Trans, A Phys Metall Mater Sci*. 2017;48(10):4803-20.
25. Piñol-Juez A, Iza-Mendia A, Gutiérrez I. δ/γ interface boundary sliding as a mechanism for strain accommodation during hot deformation in a duplex stainless steel. *Metall Mater Trans, A Phys Metall Mater Sci*. 2000;31(6):1671-7.
26. Jorge AM, Reis GS, Balancin O. Influence of the microstructure on the behavior of duplex stainless steel. *Mater Sci Eng A*. 2011;528(6):2259-64.
27. Patra S, Ghosh A, Kumar V, Chakrabarti D, Singhal LK. Deformation induced austenite formation in as-cast 2101 duplex stainless steel and its effect on hot-ductility. *Mater Sci Eng A*. 2016;660:61-70.
28. Reddy NS, Park CH, Lee YH, Lee CS. Neural network modelling of flow stress in Ti-6Al-4V alloy with equiaxed and Widmanstatten microstructures. *Mater Sci Technol*. 2008;24(3):294-301. <http://dx.doi.org/10.1179/174328408X276233>.
29. Haghdadi N, Zarei-Hanzaki A, Khalesian AR, Abedi HR. Artificial neural network modeling to predict the hot deformation behavior of an A356 aluminum alloy. *Mater Des*. 2013;49:386-91.
30. Ji G, Li F, Li Q, Li H, Li Z. A comparative study on Arrhenius-type constitutive model and artificial neural network model to predict high-temperature deformation behaviour in Aermet 100 steel. *Mater Sci Eng A*. 2011;528(13-14):4774-82.
31. Han Y, Qiao G, Sun JP, Zou D. A comparative study on constitutive relationship of as-cast 904L austenitic stainless steel during hot deformation based on Arrhenius-type and artificial neural network models. *Comput Mater Sci*. 2013;67:93-103.
32. Sun Y, Zeng W, Ma X, Xu B, Liang X, Zhang J. A hybrid approach for processing parameters optimization of Ti-22Al-25Nb alloy during hot deformation using artificial neural network and genetic algorithm. *Intermetallics*. 2011;19(7):1014-9.
33. Sun Y, Zeng WD, Zhao YQ, Qi YL, Ma X, Han YF. Development of constitutive relationship model of Ti600 alloy using artificial neural network. *Comput Mater Sci*. 2010;48(3):686-91.
34. Kumar S, Karmakar A, Nath SK. Construction of hot deformation processing maps for 9Cr-1Mo steel through conventional and ANN approach. *Mater Today Commun*. 2021;26:101903.
35. Jang J-SR. ANFIS: adaptive-network-based fuzzy inference system. *IEEE Trans Syst Man Cybern*. 1993;23(3):665-85.
36. Chen DD, Lin YC, Zhou Y, Chen MS, Wen DX. Dislocation substructures and an adaptive-network-based fuzzy inference system model for constitutive behavior of a Ni-based superalloy during hot deformation. *J Alloys Compd*. 2017;708:938-46.
37. Vafaeezhad H, Seyedein SH, Aboutalebi MR, Eivani AR. Application of constitutive description and integrated ANFIS – ICA analysis to predict hot deformation behavior of Sn-5Sb lead-free solder alloy. *J Alloys Compd*. 2017;697:287-99.
38. Sumathi S, Surekha P. A computational intelligence paradigms theory and applications using MATLAB®. New York: CRC Press; 2010.
39. Zadeh LA. Fuzzy sets. *Inf Control*. 1965;8(3):338-53.